

# Quantum confinement in oxide quantum wells

Susanne Stemmer and Andrew J. Millis

Quantum wells created from nanostructured transition metal oxides offer unique possibilities for creating and manipulating quantum states of matter, including novel superconductors, high Curie temperature magnets, controllable metal-insulator transitions, and new topological states. This article explores what is known and conjectured about confined electronic states in oxide quantum wells. Theoretical challenges are reviewed, along with issues arising in the creation of oxide quantum wells. Examples from the current experimental state of the art are summarized, open questions are discussed, and prospects for the future are outlined. The key roles of epitaxial strain and proximity effects are emphasized.

## Introduction

Quantum confinement involves the use of spatial modulations of chemical composition and electric fields to localize electrons to regions that are sufficiently small (at least in one direction) that their quantum mechanical properties are affected. Quantum wells, sketched in **Figure 1**, are basic to semiconductor science and technology.<sup>1</sup> In its simplest form, a quantum well involves a thin layer of one material, such as InGaN, sandwiched between thick layers of another (often a wider bandgap) material, such as GaN. This creates a potential well in which carriers can move in two directions but are confined in the third.

The basic ideas of quantum confinement—using a gradient of the electrochemical potential, such as band offsets, band bending, and applied fields, to localize the electrons in particular spatial regions—apply to transition metal oxides, but the physics is much richer. First and foremost, electrons in the narrow *d*-bands of transition metal oxides are subject to strong electron-electron interactions (thus the electrons are referred to as being “correlated,” and materials containing such electrons are referred to as “correlated electron materials”). The electron-electron interactions (“correlations”) lead to a rich variety of physical phenomena that can be accessed, modified, and controlled in quantum wells. Examples include magnetism with high Curie temperature, “Mott” (electron correlation-driven) metal-to-insulator transitions,

high transition temperature ( $T_c$ ) superconductivity, and unique charge and magnetic order.

The electron densities required to obtain the Mott insulator and many of the related correlation-driven effects are typically very high, on the order of one electron per  $10^{22}$   $\text{cm}^{-3}$ , or a sheet carrier density of several  $10^{14}$   $\text{cm}^{-2}$  in a single atomic plane.<sup>2</sup> Such sheet carrier densities are an order of magnitude higher than the highest density two-dimensional electron gases (2DEGs) achievable in conventional semiconductors (the III-nitrides). One of the unique aspects of oxide quantum wells is that these densities can be achieved.<sup>3–5</sup> The article by Hilgenkamp in this issue discusses one example of such an interface, namely that between the band insulators  $\text{LaAlO}_3$  and  $\text{SrTiO}_3$ . In this article, we discuss the issues arising in the theoretical description of new high density oxide quantum wells, describe some aspects of the materials, fabrication techniques and diagnostics used, and discuss a few prototypical examples at the forefront of current research interests.

## Theoretical challenges

Theoretical and practical challenges arise for high electron density quantum wells. The high carrier densities imply that the physics can be much more local than in conventional semiconductors, because the interelectron distances become comparable to the distances between atoms in the crystal lattice. Materials must be controlled on subnanometer length

Susanne Stemmer, Materials Department, University of California, Santa Barbara, CA; stemmer@mrl.ucsb.edu  
Andrew J. Millis, Department of Physics, Columbia University, NY; millis@phys.columbia.edu  
DOI: 10.1557/mrs.2013.265

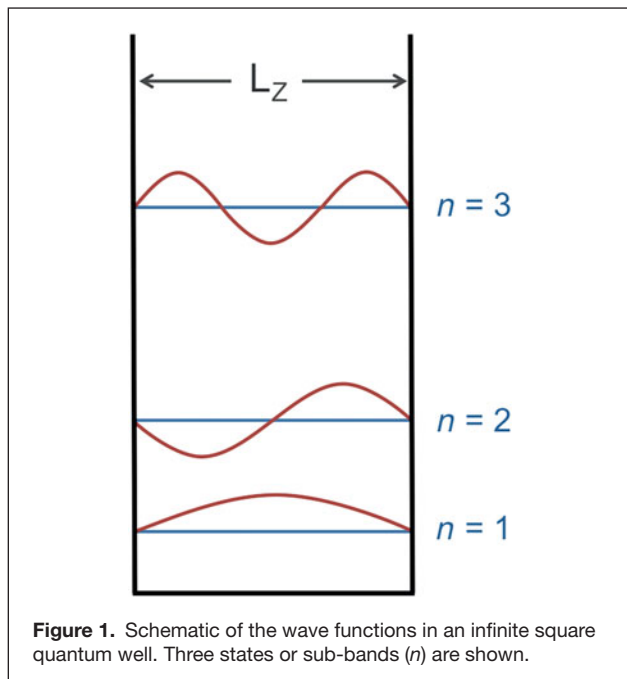


**Figure 1.** Schematic of the wave functions in an infinite square quantum well. Three states or sub-bands ( $n$ ) are shown.

scales, and the specifics of the interface are important. The richer physics means that information beyond just the spatial extent of the electron wave function is needed.

In conventional semiconductors, electron-electron interactions may, to a good approximation, be neglected (except for the electrostatic potential variations produced by spatially varying charge distributions). The situation may be discussed in terms of the electron wave function, which obeys the single-particle Schrödinger equation appropriate for a particle moving in a spatially varying potential,  $V$ . Further, the electron densities are typically low enough that an effective mass or  $\mathbf{k}\cdot\mathbf{p}$  approximation may be made for the electronic band structure (this has been done in Equation 1). For the simple quantum well sketched in Figure 1, the physics may thus be encapsulated in a Schrödinger equation of the form:

$$\begin{aligned}
 -\frac{\hbar^2}{2m^*} \frac{d^2 \psi_n(z, k_{\perp})}{dz^2} + V(z) \psi_n(z, k_{\perp}) \\
 = \left( E_n + \frac{\hbar^2 k_{\perp}^2}{2m^*} \right) \psi_n(z, k_{\perp}).
 \end{aligned}
 \quad (1)$$

Here  $k_{\perp}$  is the wave vector corresponding to motion transverse to the interfaces separating the two materials,  $z$  is the coordinate perpendicular to the interface, and the index  $n$  labels discrete states of motion transverse to the interfaces. Solutions of different  $n$  are referred to as sub-bands. If for some  $n$  the wave functions vanish as  $z$  goes to  $\pm\infty$  (so  $E_n$  is less than the value of  $V$  far from the well), it can be stated that sub-band  $n$  is confined in the direction transverse to the interface. Quantum confinement refers to the situation when only a few sub-bands are occupied.

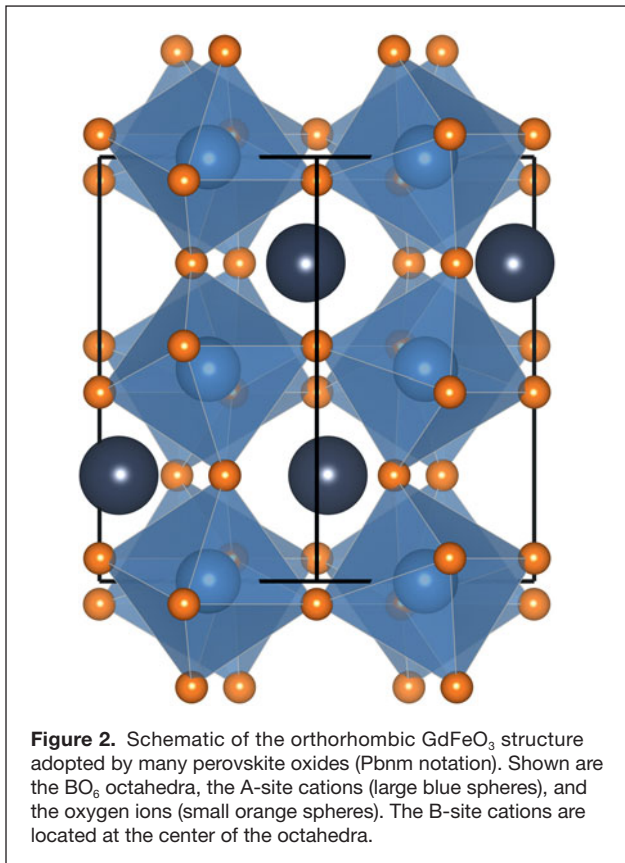
In transition metal oxides, the relevant electronic states are the transition metal  $d$  orbitals, which are highly spatially compact (typically  $0.5 \text{ \AA}$  compared to the  $\sim 4 \text{ \AA}$  spacing between transition metal ions) and are delocalized only via their overlap with ligand orbitals (typically oxygen  $2p$ ); thus the  $\mathbf{k}\cdot\mathbf{p}$  approximation is not generally relevant. The high density and small size of the  $d$  orbital means that the interesting physics is to a large degree driven by a short range (effectively onsite) Coulomb interaction. In transition metal ions in free space, the  $d$ -levels occur in groups of five degenerate (equal energy) states. The degeneracy may be partially or fully lifted in crystals, so that different  $d$ -states may have different energies and therefore occupancies. The orbital occupancies are controlled by symmetry-breaking electric fields, transition metal-oxygen bond lengths, and octahedral rotations and strongly affect the physics. Bond angles play a very important role in correlated electron physics and may be controlled by judicious choice of interface materials.

To model the correlated situation, one must go beyond Equation 1 and consider a many-body Green function, which depends on orbital and spin as well as position transverse to the interface and momentum along it, and contains information about many-body effects such as magnetic, superconducting, and Mott insulating states. Even on a very basic level, the calculation of confining potentials is on a much less firm theoretical footing for correlated oxides, because the band offsets are determined by the energies of the frontier orbitals, which are set, in part, by beyond-band theory correlations.<sup>6</sup> Systematic investigations of these and related issues remain for the future.

### Materials

Transition metal oxides crystallize in many structures, but to date, the experimental community has largely concentrated on quantum wells made from materials such as  $R\text{TiO}_3$ ,  $\text{SrTiO}_3$ ,  $\text{SrVO}_3$ , and  $R\text{NiO}_3$  ( $R$  is a trivalent rare-earth ion, including Y). These materials crystallize in perovskite-derived (chemical formula:  $\text{ABO}_3$ ) structures. The B site ion in  $\text{ABO}_3$  is a transition metal with a partially filled (empty in case of  $\text{SrTiO}_3$ )  $d$ -shell and is octahedrally coordinated with six oxygen ions, while the A site ion is typically an alkali earth (Ca, Sr, or Ba) or a trivalent rare-earth ion, including Y.

The A site ion affects the electronic properties in two ways. First, via filling of the  $d$ -shell: Sr or Ba donates two electrons, while Y, La, or other lanthanides ( $R$ ) donate three so that the nominal configuration of  $\text{SrVO}_3$  is  $d^1$ , while that of  $\text{LaVO}_3$  or  $\text{YVO}_3$  is  $d^2$ . Second, via internal strains, if the chemically preferred A-O distance is smaller (larger) than  $\sqrt{2}$  times the B-O distance, the B-O complex will be subject to compressive (tensile) strain.<sup>7</sup> Compressive internal strains are common and lead to rotational distortions, relative to the ideal cubic perovskite structure.<sup>7-9</sup> A prominent example, the orthorhombic  $\text{GdFeO}_3$  structure (space group  $\text{Pbnm}$ ), is shown in **Figure 2**.  $\text{BO}_6$  rotations and distortions couple strongly to electronic properties both by changing bandwidths and by lifting degeneracies in the  $d$ -shell.



The rare-earth nickelates ( $\text{RNiO}_3$ ) and the rare-earth titanates ( $\text{RTiO}_3$ ) are two prototypical perovskite oxides illustrating the close relationship between properties, oxygen octahedral tilts/distortions, and orbital ordering or polarizations. In the  $\text{RNiO}_3$  series, the temperature of the metal-to-insulator transition systematically increases with increasing deviation of the Ni–O–Ni bond angle from the ideal  $180^\circ$  angle in the cubic perovskite structure.<sup>10</sup> The  $\text{RTiO}_3$  series are prototype Mott insulators, with a single electron occupying the Ti  $t_{2g}$  orbitals. Magnetic ordering in the  $\text{RTiO}_3$  is closely coupled with Ti–O octahedral tilts and distortions, which remove the orbital degeneracy,<sup>11–13</sup> often via long-range ferro-orbital or antiferro-orbital ordering.<sup>14–18</sup>

In thin films and heterostructures, octahedral tilts are modified by epitaxial coherency strains and by interfacial coupling (connectivity) to adjacent layers or the substrate. The close coupling of tilts to orbital polarization and properties influences the phenomena observed in ultrathin oxide quantum wells, as will be further discussed later. In recent years, methods have been developed to establish octahedral tilt patterns as a function of epitaxial lattice mismatch strain even in few atomic layer thick films and superlattices;<sup>19–28</sup> an excellent review of this subject has recently appeared in *MRS Bulletin*.<sup>29</sup>

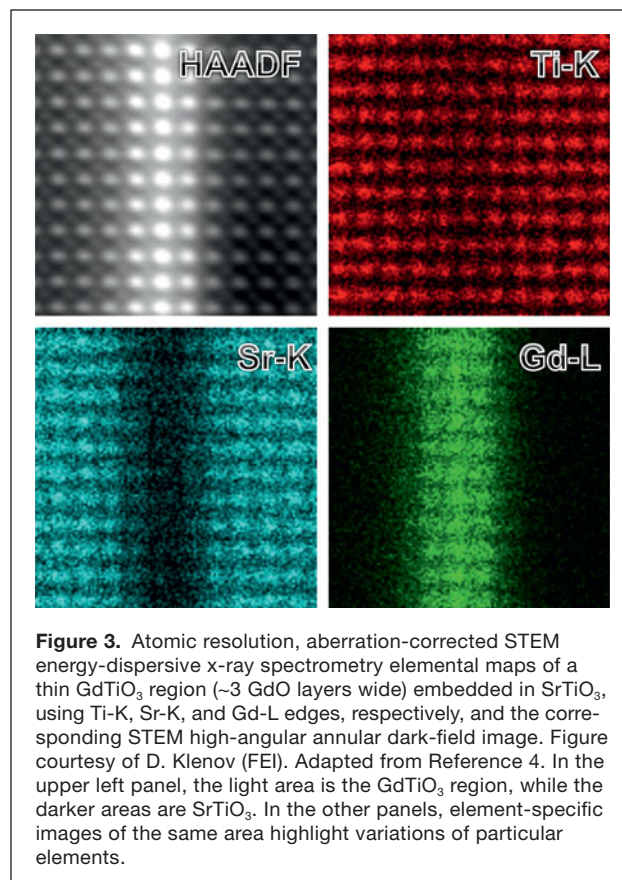
Quantum wells are created by a spatial variation of the electrochemical potential. This may be accomplished in several ways. One is by varying the A-site ion, for example by sandwiching a few layers of  $\text{LaMnO}_3$  between layers of  $\text{SrMnO}_3$ . The difference in charge between La (3+) and Sr (2+) ions

creates a spatially varying electric potential, which can cause a spatially varying electron density. A second choice is to vary the B-site ion, for example by sandwiching a few layers of  $\text{SrVO}_3$  between layers of  $\text{SrTiO}_3$ . In this example, the different electronegativities of V and Ti define the quantum well.

Most of the quantum wells studied to date have been grown on (001) planes (using [pseudo] cubic notation), although (111) structures have been theoretically discussed<sup>30,31</sup> as giving rise to interesting topological properties.

### Fabrication and diagnostics

A number of different deposition methods are currently being used to fabricate oxide quantum structures (for a review, see Reference 32). Addressing challenges such as stoichiometry control<sup>33,34</sup> and defects created by energetic deposition (pulsed laser deposition [PLD], sputtering<sup>35</sup>) remains critical and is non-trivial. Advanced transmission electron microscopy techniques, in particular those based on scanning transmission electron microscopy (STEM), provide quantitative information about interfacial chemical abruptness.<sup>36,37</sup> An example is shown in **Figure 3**. Unit-cell resolved studies of  $\text{BO}_6$  rotations and bond-length changes are more challenging, even with the most advanced aberration-corrected transmission electron microscopes. A recently developed technique is position averaged convergent beam electron diffraction (PACBED)<sup>38</sup> in STEM, which is sensitive to picometer-scale structural



distortions,<sup>39</sup> has unit cell spatial resolution, and has been used to quantify oxygen octahedral tilts at interfaces and in superlattices.<sup>27,28</sup>

Transport and device characteristics, including carrier mobilities, magnetic ordering temperatures, unintentional charge carriers, or, conversely, charge carrier densities that are lower than the expected concentrations, are the most sensitive measure of material quality. Disorder can give rise to carrier localization unrelated to true correlation physics.<sup>40</sup> For example, in SrTiO<sub>3</sub>, unintentional carriers can be due to oxygen vacancies, while unintentional acceptors (such as Sr vacancies) act as charge traps. Doping studies and measurements of carrier mobilities have demonstrated the excellent materials quality that can be achieved by oxide molecular beam epitaxy.<sup>41</sup> Careful control of growth parameters in PLD allowed for the synthesis of superconducting Sr<sub>2</sub>RuO<sub>4</sub> films.<sup>42</sup> The particular properties of strongly correlated materials, such as low carrier mobilities and high electrical resistances, add extra challenges to characterizing material quality and electronic structure using transport properties.

### Examples of oxide quantum well studies SrTiO<sub>3</sub>/SrVO<sub>3</sub>/SrTiO<sub>3</sub>

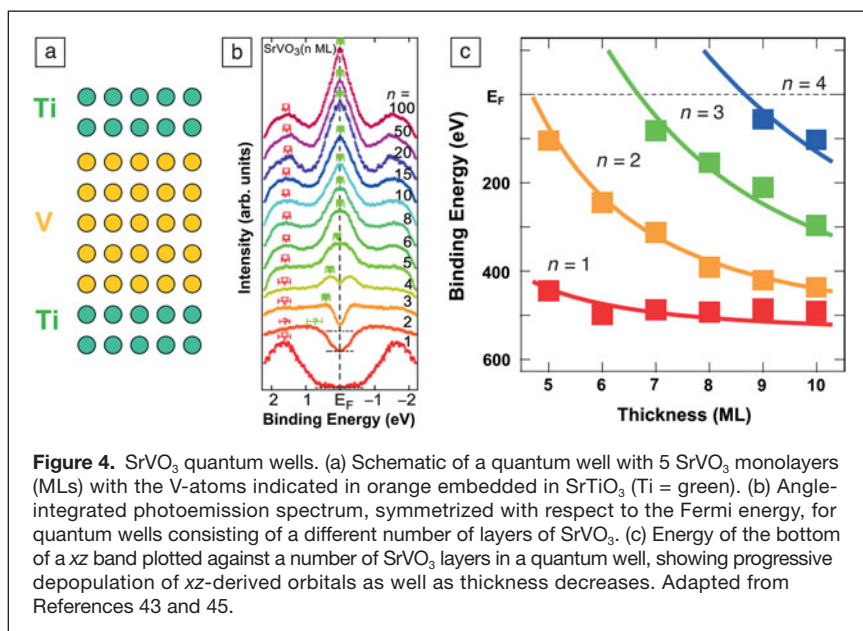
Yoshimatsu et al.<sup>43–45</sup> used photoemission (a technique based on the photoelectric effect in which the energies and momenta of electrons emitted in response to incident light are analyzed to obtain information about the occupied electronic states in a material) to study quantum wells consisting of  $n$  layers of SrVO<sub>3</sub> (a moderately correlated metal crystallizing in the ideal cubic perovskite structure) embedded in SrTiO<sub>3</sub> (a cubic perovskite band insulator), see schematic in **Figure 4a**. The vanadium ion is nominally in the  $d^1$  configuration, and in the cubic bulk material, the one  $d$ -electron is shared between the three  $t_{2g}$  symmetry  $d$  orbitals,  $d_{xy}$ ,  $d_{xz}$ ,  $d_{yx}$ . To a first

approximation, an electron in the  $d_{xy}$  orbital can move easily in the  $x$ - $y$  plane but has only a very weak dispersion in the  $z$  direction.

Figure 4b shows the photoemission spectra (many-body density of states) for quantum wells of a varying number of SVO layers. Photoemission measures the occupied portion of the electronic density of states; this figure has been symmetrized in energy. One sees that down to approximately six unit cells, the spectrum remains quite similar to that of the bulk material. Below this thickness, changes become apparent—first a suppression of the density of states peak at the Fermi level, then the appearance of a suppression (pseudogap), then the appearance of a full gap for two unit cells, which becomes much larger in magnitude for  $n = 1$ . Many oxide quantum wells and ultrathin films exhibit a metal-insulator transition when the film thickness is decreased below a few unit cells.<sup>45–50</sup> The spectroscopic evidence for gap formation suggests an intrinsic origin (as opposed to disorder causing localization).

Figure 4c shows that these effects occur in parallel with a thickness dependent orbital polarization effect, whereby the  $xz$  and  $yz$  bands (shown in the figure), which involve motion transverse to the interface, get progressively pushed upward in energy. As  $n$  approaches 1, what remains is a small number of  $xy$  bands (not shown) that become insulating. Also interestingly, this experiment reports no evidence for any leakage of electrons in SrVO<sub>3</sub> into the SrTiO<sub>3</sub> region. The quantum well evidently provides essentially complete confinement.

The SrVO<sub>3</sub> quantum well, along with many other experiments, shows that quantum confinement can qualitatively alter the electronic properties, but confinement effects become detectable only at very short length scales, in this case, films with less than six unit cell thickness.



### LaMnO<sub>3</sub>/SrMnO<sub>3</sub> superlattices

**Figure 5** shows a schematic of an electrostatically (A-site) defined set of quantum wells of alternating layers of LaMnO<sub>3</sub> and SrMnO<sub>3</sub>. The different ionic charges of La and Sr mean that in bulk LaMnO<sub>3</sub>, the nominal Mn configuration is  $d^4$ , while in bulk SrMnO<sub>3</sub>, it is  $d^3$ . SrMnO<sub>3</sub> crystallizes in the cubic perovskite structure and is a simple Neel (two sublattice) antiferromagnet, while LaMnO<sub>3</sub> exhibits a strong Jahn–Teller distortion that organizes the size Mn–O bonds into three inequivalent pairs with bond lengths ranging from 2.07 to 1.95 Å. This leads to a layered antiferromagnetic structure consisting of ferromagnetic planes with alternating spin orientations.

Santos and co-workers<sup>51</sup> fabricated quantum well superlattices of this type and used neutron reflectometry to extract the space-dependent magnetic moment. Neutron reflectometry is a



transport and other properties, as they may be at the core of many observed phenomena.

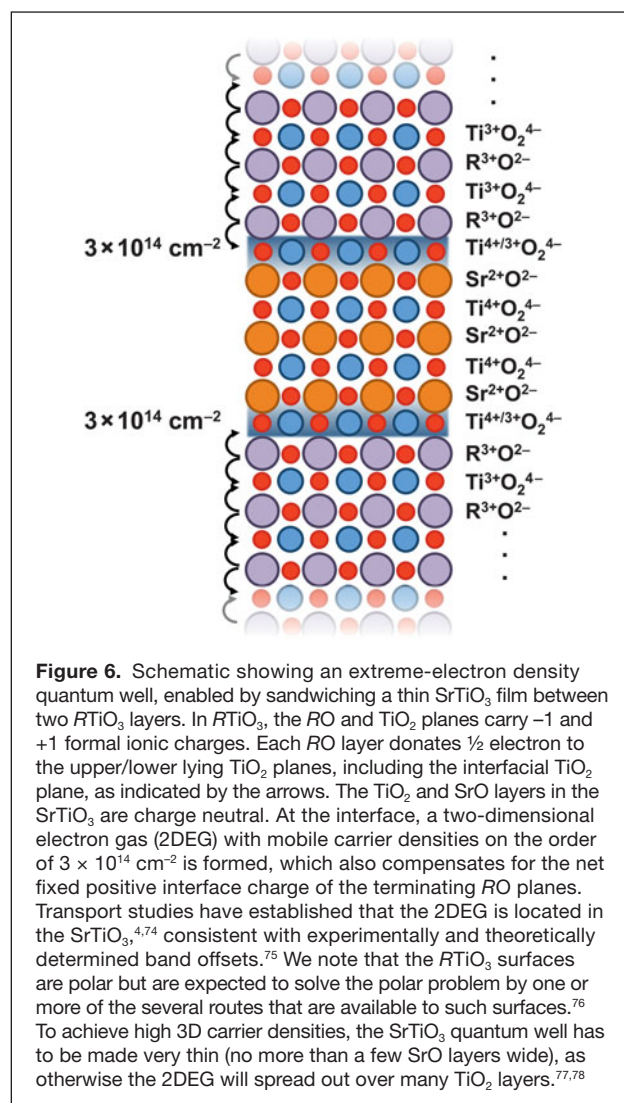
### *SrTiO<sub>3</sub> quantum wells with extreme electron densities*

Two-dimensional electron gases at interfaces between SrTiO<sub>3</sub> and RTiO<sub>3</sub> exhibit *mobile* carrier densities of several  $10^{14}$  cm<sup>-2</sup>.<sup>3,4</sup> These extreme electron densities are introduced into the *d*-bands of SrTiO<sub>3</sub>, a material that is a band insulator in the bulk (i.e., *not* a correlated material). The ideal RTiO<sub>3</sub>/SrTiO<sub>3</sub> interface contains  $\frac{1}{2}$  electron per cubic interface unit cell (or  $3.5 \times 10^{14}$  cm<sup>-2</sup>), which, even if these carriers are confined to a single interfacial TiO<sub>2</sub> plane, is half the density required for a Mott insulator, namely one electron per 3D unit cell (or  $7 \times 10^{14}$  cm<sup>-2</sup> per TiO<sub>2</sub> plane). Fortunately, RTiO<sub>3</sub>/SrTiO<sub>3</sub> interfaces are symmetric, that is, both types of interfaces, RTiO<sub>3</sub> on SrTiO<sub>3</sub> and SrTiO<sub>3</sub> on RTiO<sub>3</sub>, provide  $\frac{1}{2}$  electron per cubic interface unit cell.<sup>4,66</sup> Quantum wells that are bound by two such interfaces contain electron densities of  $7 \times 10^{14}$  cm<sup>-2</sup>, spread out over the width of the quantum well, which has to be made very narrow to achieve high 3D electron densities (**Figure 6**).

Signatures of mass enhancement were observed in the DC transport of extreme-density quantum wells of SrTiO<sub>3</sub> sandwiched between the Mott insulator GdTiO<sub>3</sub> that was on the verge to a transition to an insulator.<sup>66</sup> Such mass enhancement is similar to what is observed in doped (metallic) bulk RTiO<sub>3</sub> near the Mott transition.<sup>67</sup> At a critical thickness (2 SrO layers), or 3D electron density, a correlated insulating state emerges (**Figure 7a**).<sup>66</sup> Using atomic resolution STEM, it was shown that orthorhombic-like Sr-site displacements (which are closely coupled with oxygen octahedral tilts) are observed only for SrTiO<sub>3</sub> quantum wells that were 1 and 2 SrO layers wide,<sup>68</sup> in precise agreement with the observed metal-to-insulator transition (**Figure 7b**). Metallic quantum wells (those thicker than 2 SrO layers) showed no Sr displacements and octahedral tilts.<sup>68</sup> Therefore, similar to bulk Mott insulators, the transition to the insulating state is accompanied by a reduction in symmetry. These results support true “Mott” physics, controlled by the combination of on-site repulsive interaction at large electron densities and structural distortions in these quantum wells.

Recent theoretical studies of quantum wells of 1 SrO layer in GdTiO<sub>3</sub> suggest the formation of a dimer Mott insulator state, in which electrons are localized to bonding orbitals on molecular dimers formed across a bilayer of two TiO<sub>2</sub> planes.<sup>69</sup> These calculations were carried out for a different crystallographic orientation relationship than the experiments, and thus a complete theoretical understanding of the experimentally observed insulating state is still lacking. Alternative routes to an insulating state, such as charge ordering, may exist.

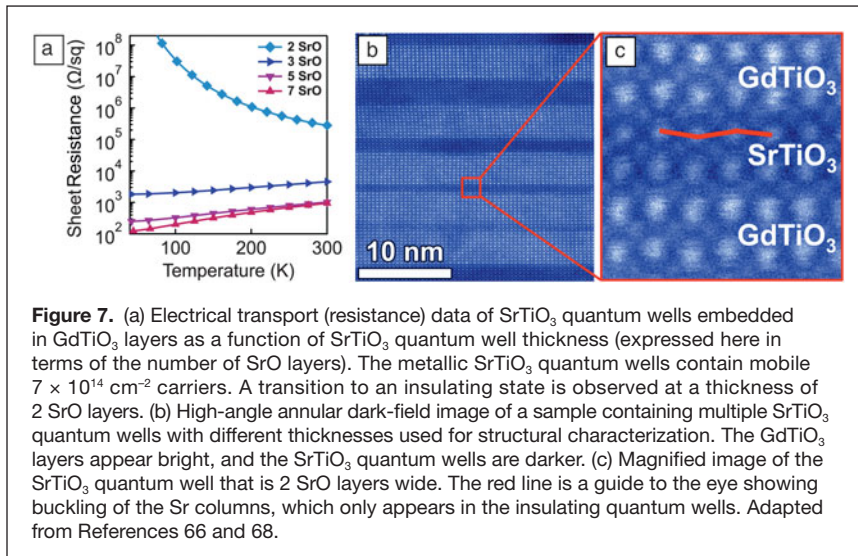
In addition to the polar/nonpolar interfaces described previously, modulation doping can be used to introduce large densities of carriers into such quantum wells.<sup>70,71</sup> Moreover, by judicious use of the materials that interface the quantum well, octahedral tilts and other properties may be controlled. For example, in the experiments described previously, the



quantum well was bound by GdTiO<sub>3</sub>, which is among the more strongly distorted RTiO<sub>3</sub>s, and is also an insulating ferromagnet (magnetic moment directions alternate from layer to layer but net magnetic moment remains, unlike in antiferromagnetic materials). Not only does this give rise to fairly large distortions in the insulating SrTiO<sub>3</sub> quantum wells, but also to ferromagnetism in the metallic quantum wells below a critical thickness.<sup>72</sup>

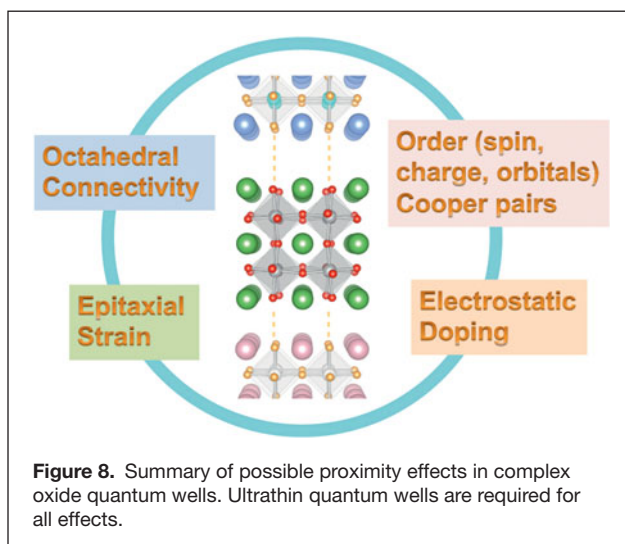
### Conclusions and future outlook

Combining spatially resolved studies of structural distortions and orbital polarization with measurements of properties (such as magnetism and electrical transport) should allow for addressing some of the most interesting and challenging scientific questions in the field of strongly correlated materials physics and electronics. In particular, it will be important to determine if the orbital/structural/bandwidth control afforded by proximity effects in heterostructures can be used to (1) rationally engineer emergent states (beyond metal-insulator transitions);<sup>29</sup>



(2) bring strongly correlated oxides closer to quantum phase transitions to allow for electric field control of correlated phenomena; and (3) conduct systematic studies that distinguish the relative roles of orbital coupling to the lattice and electron-electron interactions in correlated materials physics and phenomena.

**Figure 8** illustrates the different routes to control strongly correlated materials using narrow quantum wells and interfacial proximity effects. Specifically, structural distortions, high electron (or hole) densities introduced by electrostatic doping, and a host of properties, such as ferromagnetism and superconductivity, can be induced in high-quality epitaxial structures. Such hybrid and proximity effects are likely to be of great interest for applications in spintronics, quantum computing, as a route to Majorana fermions (novel quantum states, which, unlike electrons, are their own antiparticles and that have been proposed as a substrate for quantum computing applications), and, more generally, for artificially designing



novel states of matter that do not exist in bulk. Modulating extreme carrier densities by field effect could also be of great interest for RF transistors<sup>73</sup> or tunable plasmonic devices. Ultrathin layers are necessary, requiring exquisite control not only over atomic layers but also of defects and doping, to avoid artifacts from localization due to disorder. Advances in theoretical understanding are also needed. The theoretical and experimental results achieved to date demonstrate that the exciting possibility of using oxide quantum wells to design correlation physics from the bottom up is now becoming a reality.

### Acknowledgments

S.S. would like to acknowledge discussions and collaborations with Jim Allen, Leon Balents, Pouya Moetakef, Clayton Jackson, Dmitri Klenov, Jack Zhang, Jinwoo Hwang, Junwoo Son, Chris Van de Walle, Anderson Janotti, Siddharth Rajan, David Goldhaber-Gordon, and Jimmy Williams. She also thanks Adam Kajdos, Jack Zhang, Jinwoo Hwang, and Clayton Jackson for help with some of the figures for this article. Work at UCSB was supported by the Army Research Office (Grant No. W911-NF-09-1-0398), the US National Science Foundation (Grant Nos. DMR-1006640 and DMR-1121053), the US Department of Energy (Award No. DE-FG02-02ER45994), and DARPA (Award No. W911NF-12-1-0574). A.J.M. thanks Hanghui Chen, Hung Dang, M.J. Han, Chungwei Lin, Peter Littlewood, Chris Marianetti, Satoshi Okamoto, Hyowon Park, Seyoung Park, Darrell Schlom, and Jean-Marc Triscone for collaborations and discussions and the US Department of Energy (Award No. DOE-FG-BES2-04ER46169) and the US Army Research Office (Award W911NF-09-1-0345) for support.

### References

1. C. Weisbuch, B. Vinter, *Quantum Semiconductor Structures* (Academic Press, San Diego, 1991).
2. C.H. Ahn, A. Bhattacharya, M. Di Ventra, J.N. Eckstein, C.D. Frisbie, M.E. Gershenson, A.M. Goldman, I.H. Inoue, J. Mannhart, A.J. Millis, A.F. Morpurgo, D. Natelson, J.-M. Triscone, *Rev. Mod. Phys.* **78**, 1185 (2006).
3. J.S. Kim, S.S.A. Seo, M.F. Chisholm, R.K. Kremer, H.U. Habermeier, B. Keimer, H.N. Lee, *Phys. Rev. B* **82**, 201407 (2010).
4. P. Moetakef, T.A. Cain, D.G. Ouellette, J.Y. Zhang, D.O. Klenov, A. Janotti, C.G. Van de Walle, S. Rajan, S.J. Allen, S. Stemmer, *Appl. Phys. Lett.* **99**, 232116 (2011).
5. N. Nakagawa, H.Y. Hwang, D.A. Muller, *Nat. Mater.* **5**, 204 (2006).
6. J. Zaanen, G.A. Sawatzky, J.W. Allen, *Phys. Rev. Lett.* **55**, 418 (1985).
7. P.M. Woodward, *Acta Crystallogr., Sect. B: Struct. Sci* **53**, 44 (1997).
8. P.M. Woodward, *Acta Crystallogr., Sect. B: Struct. Sci* **53**, 32 (1997).
9. A.M. Glazer, *Acta Crystallogr., Sect. B: Struct. Sci* **28**, 3384 (1972).
10. J.B. Torrance, P. Lacorre, A.I. Nazzari, E.J. Ansaldo, C. Niedermayer, *Phys. Rev. B* **45**, 8209 (1992).
11. J.B. Goodenough, J.S. Zhou, *J. Mater. Chem.* **17**, 2394 (2007).
12. E. Pavarini, A. Yamasaki, J. Nuss, O.K. Andersen, *New J. Phys.* **7**, 1 (2005).
13. M. Mochizuki, M. Imada, *New J. Phys.* **6**, 154 (2004).
14. M. Itoh, M. Tsuchiya, H. Tanaka, K. Motoya, *J. Phys. Soc. Jpn.* **68**, 2783 (1999).
15. J. Akimitsu, H. Ichikawa, N. Eguchi, T. Miyano, M. Nishi, K. Kakurai, *J. Phys. Soc. Jpn.* **70**, 3475 (2001).
16. H. Nakao, Y. Wakabayashi, T. Kiyama, Y. Murakami, M. von Zimmermann, J.P. Hill, D. Gibbs, S. Ishihara, Y. Taguchi, Y. Tokura, *Phys. Rev. B* **66**, 184419 (2002).

17. R. Schmitz, O. Entin-Wohlman, A. Aharony, A.B. Harris, E. Muller-Hartmann, *Phys. Rev. B* **71**, 144412 (2005).
18. E. Pavarini, S. Biermann, A. Poteryaev, A.I. Lichtenstein, A. Georges, O.K. Andersen, *Phys. Rev. Lett.* **92**, 176403 (2004).
19. F.Z. He, B.O. Wells, Z.G. Ban, S.P. Alpay, S. Grenier, S.M. Shapiro, W.D. Si, A. Clark, X.X. Xi, *Phys. Rev. B* **70**, 235405 (2004).
20. A. Vaillonis, H. Boschker, W. Siemons, E.P. Houwman, D.H.A. Blank, G. Rijnders, G. Koster, *Phys. Rev. B* **83**, 064101 (2011).
21. S.J. May, J.W. Kim, J.M. Rondinelli, E. Karapetrova, N.A. Spaldin, A. Bhattacharya, P.J. Ryan, *Phys. Rev. B* **82**, 014110 (2010).
22. C.L. Jia, S.B. Mi, M. Faley, U. Poppe, J. Schubert, K. Urban, *Phys. Rev. B* **79**, 081405 (2009).
23. H. Rotella, U. Luder, P.E. Janolin, V.H. Dao, D. Chateigner, R. Feyerherm, E. Dudzik, W. Prellier, *Phys. Rev. B* **85**, 184101 (2012).
24. S.J. May, C.R. Smith, J.W. Kim, E. Karapetrova, A. Bhattacharya, P.J. Ryan, *Phys. Rev. B* **83**, 153411 (2011).
25. A. Borisevich, O.S. Ovchinnikov, H.J. Chang, M.P. Oxley, P. Yu, J. Seidel, E.A. Eliseev, A.N. Morozovska, R. Ramesh, S.J. Pennycook, *ACS Nano* **4**, 6071 (2010).
26. J. He, A. Borisevich, S.V. Kalinin, S.J. Pennycook, S.T. Pantelides, *Phys. Rev. Lett.* **105**, 227203 (2010).
27. J. Hwang, J. Son, J.Y. Zhang, A. Janotti, C.G. Van de Walle, S. Stemmer, *Phys. Rev. B* **87**, 060101 (2013).
28. J. Hwang, J.Y. Zhang, J. Son, S. Stemmer, *Appl. Phys. Lett.* **100**, 191909 (2012).
29. J.M. Rondinelli, S.J. May, J.W. Freeland, *MRS Bull.* **37**, 261 (2012).
30. K.Y. Yang, W.G. Zhu, D. Xiao, S. Okamoto, Z.Q. Wang, Y. Ran, *Phys. Rev. B* **84**, 201104 (2011).
31. A. Ruegg, G.A. Fiete, *Phys. Rev. B* **84**, 201103 (2011).
32. A.B. Posadas, M. Lippmaa, F.J. Walker, M. Dawber, C.H. Ahn, J.M. Triscone, in *Physics of Ferroelectrics: A Modern Perspective*, K.M. Rabe, C.H. Ahn, J.M. Triscone, Eds. (Springer-Verlag, Berlin, 2007), vol. **105**, pp. 219–304.
33. T. Ohnishi, K. Shibuya, T. Yamamoto, M. Lippmaa, *J. Appl. Phys.* **103**, 103703 (2008).
34. B. Jalan, P. Moetafak, S. Stemmer, *Appl. Phys. Lett.* **95**, 032906 (2009).
35. J.J. Cuomo, J.P. Doyle, J. Bruley, J.C. Liu, *Appl. Phys. Lett.* **58**, 466 (1991).
36. L.F. Kourkoutis, H.L. Xin, T. Higuchi, Y. Hotta, J.H. Lee, Y. Hikita, D.G. Schlom, H.Y. Hwang, D.A. Muller, *Philos. Mag.* **90**, 4731 (2010).
37. S.J. Pennycook, M.F. Chisholm, A.R. Lupini, M. Varela, A.Y. Borisevich, M.P. Oxley, W.D. Luo, K. van Benthem, S.H. Oh, D.L. Sales, *Philos. Trans. R. Soc. London, Ser. A* **367**, 3709 (2009).
38. J.M. LeBeau, S.D. Findlay, L.J. Allen, S. Stemmer, *Ultramicroscopy* **110**, 118 (2010).
39. J.M. LeBeau, A.J. D'Alfonso, N.J. Wright, L.J. Allen, S. Stemmer, *Appl. Phys. Lett.* **98**, 052904 (2011).
40. P.A. Lee, T.V. Ramakrishnan, *Rev. Mod. Phys.* **57**, 287 (1985).
41. J. Son, P. Moetafak, B. Jalan, O. Bierwagen, N.J. Wright, R. Engel-Herbert, S. Stemmer, *Nat. Mater.* **9**, 482 (2010).
42. Y. Krockenberger, M. Uchida, K.S. Takahashi, M. Nakamura, M. Kawasaki, Y. Tokura, *Appl. Phys. Lett.* **97**, 082502 (2010).
43. K. Yoshimatsu, T. Okabe, H. Kumigashira, S. Okamoto, S. Aizaki, A. Fujimori, M. Oshima, *Phys. Rev. Lett.* **104**, 147601 (2010).
44. K. Yoshimatsu, K. Horiba, H. Kumigashira, T. Yoshida, A. Fujimori, M. Oshima, *Science* **333**, 319 (2011).
45. K. Yoshimatsu, E. Sakai, M. Kobayashi, K. Horiba, T. Yoshida, A. Fujimori, M. Oshima, H. Kumigashira, *Phys. Rev. B* **88**, 115309 (2013).
46. A.X. Gray, A. Janotti, J. Son, J.M. LeBeau, S. Ueda, Y. Yamashita, K. Kobayashi, A.M. Kaiser, R. Sutar, H. Wadati, G.A. Sawatzky, C.G. Van de Walle, S. Stemmer, C.S. Fadley, *Phys. Rev. B* **84**, 075104 (2011).
47. J. Son, P. Moetafak, J.M. LeBeau, D. Ouellette, L. Balents, S.J. Allen, S. Stemmer, *Appl. Phys. Lett.* **96**, 062114 (2010).
48. R. Scherwitzl, S. Gariglio, M. Gabay, P. Zubko, M. Gibert, J.M. Triscone, *Phys. Rev. Lett.* **106**, 246403 (2011).
49. J. Liu, M. Kareev, D. Meyers, B. Gray, P. Ryan, J.W. Freeland, J. Chakhalian, *Phys. Rev. Lett.* **109**, 107402 (2012).
50. A.V. Boris, Y. Matiks, E. Benckiser, A. Frano, P. Popovich, V. Hinkov, P. Wochner, M. Castro-Colin, E. Detemple, V.K. Malik, C. Bernhard, T. Prokscha, A. Suter, Z. Salman, E. Morenzoni, *Science* **332**, 937 (2011).
51. T.S. Santos, B.J. Kirby, S. Kumar, S.J. May, J.A. Borchers, B.B. Maranville, J. Zarestky, S. Velthuis, J. van den Brink, A. Bhattacharya, *Phys. Rev. Lett.* **107**, 167202 (2011).
52. S. Okamoto, A.J. Millis, *Nature* **428**, 630 (2004).
53. S. Okamoto, A.J. Millis, N.A. Spaldin, *Phys. Rev. Lett.* **97**, 056802 (2006).
54. J. Chaloupka, G. Khaliullin, *Phys. Rev. Lett.* **100**, 016404 (2008).
55. P. Hansmann, X.P. Yang, A. Toschi, G. Khaliullin, O.K. Andersen, K. Held, *Phys. Rev. Lett.* **103**, 016401 (2009).
56. M. Wu, E. Benckiser, M.W. Haverkort, A. Frano, Y. Lu, N. Nwanko, S. Brück, P. Audehm, E. Goering, S. Mache, V. Hinkov, P. Wochner, G. Christiani, S. Heinze, G. Logvenov, H.-U. Habermeier, B. Keimer, *Phys. Rev. B* **88**, 125124 (2013).
57. A. Frano, E. Schierle, M.W. Haverkort, Y. Lu, M. Wu, S. Blanco-Canosa, U. Nwankwo, A.V. Boris, P. Wochner, G. Christiani, H.U. Habermeier, G. Logvenov, V. Hinkov, E. Benckiser, E. Weschke, B. Keimer, *Phys. Rev. Lett.* **111**, 106804 (2013).
58. M.J. Han, X. Wang, C.A. Marianetti, A.J. Millis, *Phys. Rev. Lett.* **107**, 206804 (2011).
59. D.G. Ouellette, S. Lee, J. Son, S. Stemmer, L. Balents, A.J. Millis, S.J. Allen, *Phys. Rev. B* **82**, 165112 (2010).
60. M.K. Stewart, D. Brownstead, J. Liu, M. Kareev, J. Chakhalian, D.N. Basov, *Phys. Rev. B* **86**, 205102 (2012).
61. M.L. Medarde, *J. Phys. Condens. Matter* **9**, 1679 (1997).
62. S. Lee, R. Chen, L. Balents, *Phys. Rev. Lett.* **106**, 016405 (2011).
63. S.B. Lee, R. Chen, L. Balents, *Phys. Rev. B* **84**, 165119 (2011).
64. B. Lau, A.J. Millis, *Phys. Rev. Lett.* **110**, 126404 (2013).
65. J.A. Liu, S. Okamoto, M. van Veenendaal, M. Kareev, B. Gray, P. Ryan, J.W. Freeland, J. Chakhalian, *Phys. Rev. B* **83**, 161102 (2011).
66. P. Moetafak, C.A. Jackson, J. Hwang, L. Balents, S.J. Allen, S. Stemmer, *Phys. Rev. B* **86**, 201102(R) (2012).
67. Y. Tokura, Y. Taguchi, Y. Okada, Y. Fujishima, T. Arima, K. Kumagai, Y. Iye, *Phys. Rev. Lett.* **70**, 2126 (1993).
68. J.Y. Zhang, J. Hwang, S. Raghavan, S. Stemmer, *Phys. Rev. Lett.* **110**, 256401 (2013).
69. R. Chen, S. Lee, L. Balents, *Phys. Rev. B* **87**, 161119(R) (2013).
70. J. Son, B. Jalan, A.P. Kajdos, L. Balents, S.J. Allen, S. Stemmer, *Appl. Phys. Lett.* **99**, 192107 (2011).
71. A.P. Kajdos, D.G. Ouellette, T.A. Cain, S. Stemmer, *Appl. Phys. Lett.* **103**, 082120 (2013).
72. P. Moetafak, J.R. Williams, D.G. Ouellette, A.P. Kajdos, D. Goldhaber-Gordon, S.J. Allen, S. Stemmer, *Phys. Rev. X* **2**, 021014 (2012).
73. M. Boucherit, O.F. Shoron, T.A. Cain, C.A. Jackson, S. Stemmer, S. Rajan, *Appl. Phys. Lett.* **102**, 242909 (2013).
74. T.A. Cain, S. Lee, P. Moetafak, L. Balents, S. Stemmer, S.J. Allen, *Appl. Phys. Lett.* **100**, 161601 (2012).
75. G. Conti, A.M. Kaiser, A.X. Gray, S. Nemsak, G.K. Palsson, J. Son, P. Moetafak, A. Janotti, L. Bjaalie, C.S. Conlon, D. Eiteneer, A.A. Greer, A. Perona, A. Rattanachata, A.Y. Saw, A. Bostwick, W. Stolte, A. Hloskovsky, W. Drube, S. Ueda, K. Kobayashi, C.G. Van de Walle, S. Stemmer, C.M. Schneider, C.S. Fadley, *J. Appl. Phys.* **113**, 143704 (2013).
76. C. Noguera, *J. Phys. Condens. Matter* **12**, R367 (2000).
77. G. Khalsa, A.H. MacDonald, *Phys. Rev. B* **86**, 125121 (2012).
78. S.Y. Park, A.J. Millis, *Phys. Rev. B* **87**, 205145 (2013). □



**5<sup>th</sup> International Symposium on Growth of III-Nitrides**

The Westin, Peachtree Plaza  
Atlanta, Georgia, USA  
May 18 – 22, 2014

**ABSTRACT SUBMISSION ENDS**  
FEBRUARY 17, 2014

## CALL FOR PAPERS

**Scientific Program**

The five-day Conference will feature oral and poster presentations covering:

- III-N Bulk growth: AlN, GaN, InN
- Epitaxial growth techniques
- Ternary and quaternary alloys
- III-N nanostructures
- Defect control and surface effects
- Optical and electrical properties
- III-N magnetic and spin-related phenomena
- III-N devices: FETs, HBTs, rectifiers, LEDs, lasers, photodetectors and novel devices

For the most up-to-date information on ISGN-5, visit [www.mrs.org/isgn-5](http://www.mrs.org/isgn-5).